Modelling And Simulation of An Energy Harvester with Piezoelectric Material Using COMSOL Multiphysics 5.3

OLUWAFEMI OLAYEBI
Federal University of Petroleum Resources, Effurun. Nigeria

Abstract- ***In this work, piezoelectric cantilever energy harvesters with different materials of varying dimensions and shapes were studied. The simulations were carried out to predict the output voltage (V) across the piezoelectric layers for different piezoelectric materials and substrate materials with various shaped cantilever beams. A rectangular beam with dimension 30 mm x 5 mm x 0.16 mm, and a U-shaped beam with dimension 30 mm x 15 mm x 0.16mm in addition to an E-shaped beam with dimension 30 mm x 25 mm x 0.16 mm were examined. COMSOL Multiphysics 5.3 was used for simulation. The properties examined included; variation of the beam length and beam width concerning frequency. Also, the variation of eigen frequency with voltage was examined for the different cantilever structures. All the cantilever structures were studied at resonance frequency between 60 to 200Hz. It was observed that the E-shaped structure gave a maximum voltage of 8.792V at the eigen frequency of 0.032Hz with an applied force of 10N. The PZT 5A with Aluminum substrate demonstrates better performance in the context of voltage output and eigen frequency compared to other piezoelectric materials under study. For energy harvesting, the E-shaped cantilever structure using PZT-5A as a piezoelectric layer and Aluminum as a substrate layer gave the best result.***

Indexed Terms- ***Energy harvesting, Piezoelectric, bimorph cantilever, FEM, COMSOL Multiphysics***

I. INTRODUCTION

Due to the present environmental concerns, the need remains for a cleaner power-generation technique that allows maximum range extension with minimal environmental impact through the use of renewable energy sources and critical part to the solution will lie in promoting renewable energy technologies. Recent advances in low power electronics have provided new opportunities for the use of piezoelectric materials to power consumer electronic devices; either without the need for batteries, or in conjunction with rechargeable batteries. Typical applications include wireless sensors, wireless networks, wearable computers, cell phones, MP3 players, and other portable electronic devices. All of these system or devices require power from batteries or some other.

Energy harvesting is the collection of "free" energy that a process generates. This includes all sorts of processes, and the resulting energy could come in variety of forms and from various sources. It is desirable to use natural ambient sources to have a green world and clean from fuel-based energy. And one of these ways is by the use of piezoelectric materials which exhibit piezoelectric effect, producing electricity when stress is applied or when under deformation.

The primary aim of this study is to model and simulate a cantilever beam energy harvester considering various piezoelectric materials and different shapes and theoretically investigate the behavior of a power harvesting system of different piezoelectric materials, develop models aimed at the prediction of the power output from various shaped piezoelectric material and use COMSOL multi physics 5.3 software to simulate the models developed.

1.1 Energy Scavenging Technologies

There are a number of Energy Scavenging Technologies which include solar radiation, thermal energy in which the generated voltage and power consumption are an increasing function of the temperature difference (Vullers, et al., 2014), passive Human Power which has to do with scavenging power off the human body for use as wearable electronic devices (Wang, 2012), the most energy rich and most easily exploitable source being at the foot during heel strike and in the bending of the ball of the foot. An

example of this is the development of piezoelectric shoe inserts, active Human Power requiring the user to perform a specific power generating motion.

1.2 Piezoelectricity.

A piezoelectric substance produces an electric charge when a mechanical stress is applied (the substance is squeezed or stretched). Conversely, a mechanical deformation (the substance shrinks or expands) is produced when an electric field is applied. This effect is formed in crystals that have no center of symmetry. To explain this, we have to look at the individual molecules that make up the crystal. Each molecule has a polarization, one end is more negatively charged and the other end is positively charged, and is called a dipole. This is a result of the atoms that make up the molecule and the way the molecules are shaped. The polar axis is an imaginary line that runs through the center of both charges on the molecule. Figure 1 shows the intrinsic piezoelectric effect in lead zirconate titanate, showing the a crystallite above and below the Curie temperature TC, where the charged zirconium or titanium ion moves relative to the center position unit cell of a material.

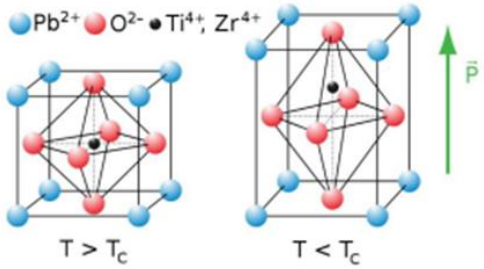

Figure 1: Intrinsic piezoelectric effect in lead zirconate titanate (Hehn & Y. Manoli, 2014)

Since this is also the most easily available transducer material, the explanation of the physical properties is limited to this material throughout this work. The Figure shows the unit cell above the Curie temperature, (left) and below the Curie temperature, (right).

1.3 Poling

A Piezoelectric material, which is non-conductive in nature, does not have free electrons, and therefore electrons cannot pass freely through the material. Piezoelectric material is made up of crystals that have many “fixed” electrons. These fixed electrons can move slightly as the crystals deform by an external force. This slight movement of electrons alters the equilibrium status in the adjacent conductive materials and creates electric force. This force will push and pull the electrons in the electrodes attached to the piezoelectric crystal as shown in the Figure 2.

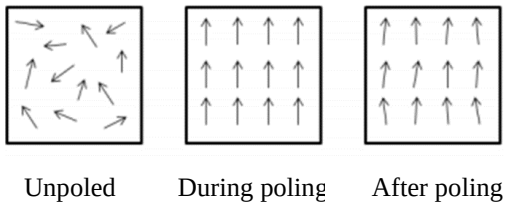

Figure 2: Alignment of electric dipoles (Datta, 2014)

Piezoelectric ceramic materials are not piezoelectric until the random ferroelectric domains are aligned. This alignment is accomplished through a process known as "poling" which means inducing a D.C. voltage across the material. The ferroelectric domains align to the induced field resulting in a net piezoelectric effect. During poling the material permanently increases in dimension between the poling electrodes and decreases in dimensions parallel to the electrodes.

The material can be depolarized by reversing the poling voltage, increasing the temperature beyond the materials Currie point, or by inducing a large mechanical stress.

1.4 Piezo-based power generation

Many piezoelectric materials have been developed over the past century, however the most common piezoelectric material is perovskite lead zirconate titanate (PZT) which contains lead and, therefore, the development of new compositions is a large and ongoing research thrust (K, 2017).

While piezoelectric ceramics are relatively affordable and provide good coupling, they are brittle and have a high density. Given the growing application of piezoelectric ceramics in microelectromechanical systems (MEMS), PZT thin films have been developed to capitalize upon the small scale to achieve flexibility, as well as the use of grain texturing (Messing, et al., 2004) and epitaxial thin films on

substrates (Isarakorn, et al., 2010) to improve coupling.

Furthermore, in order to provide compliant piezoelectric materials, piezoelectric polymers have been developed, which include polyvinylidene fluoride (PVDF), another common piezoelectric material. While piezoelectric polymers are lightweight and flexible, their coupling is considerably lower than their ceramic counterparts (Yousry, et al., 2018).

Also, (Harstad, et al., 2017) developed a new approach to improve the coupling of PVDF polymers and observed that the coupling coefficient is directly proportional to the β phase percentage in the material composition.

In a comparative study, (Shahab, et al., 2018) investigated the performance of various soft and hard piezoelectric ceramics as well as single crystal piezoelectrics which include soft PZT-5H and PZT-5A ceramics, hard PZT-4 and PZT-8 ceramics, soft piezoelectric single crystals (Lead Magnesuim Niobuim-Lead Titanate) PMN-PT and PMN-PZT, and hard manganese doped PMN-PZT (PMNPZT- Mn) materials. They showed that in off-resonance harvesting, the soft materials outperform the hard ones. They also observed that PMN-PT presented the highest electromechanical conversion efficiency. (Yang & Zu, 2016) also reported that the PZN-PT and PMN-PT single crystalline generators always outperformed PZT-based harvesters. (Hwang, et al., 2015), also developed a flexible single crystalline PMN-PZT thin film energy harvester and installed it on the heel of a combat boot. The generated power from the piezoelectric was able to power 104 LEDs during normal walking.

1.5 Piezo-based power generation applications

Energy harvesting provides continuous mechanical energy (Yang, et al., 2014) although it has one drawback which is the relatively low speed of wind near the ground due to boundary layer effects and the presence of other physical obstructions (Kishore, et al., 2014).

Flowing media offers relatively high-density kinetic energy which is usually readily available. Piezoelectric transduction can be utilized to convert the energy available in flow of both water (liquids) and air to useable electrical energy. Energy conversion from fluid flow kinetic energy to electrical energy severally reported in literature with the use of various configurations which include windmills, cantilevers, films, plates, flags, membranes, and piezo discs (Abrol & Chhabra, 2017).

1.6 Improving efficiency and power generation through piezoelectric configurations

Piezoelectric materials can be configured in many different ways that prove useful in power harvesting applications. The configuration of the power harvesting device can be changed through modification of piezoelectric materials, altering the electrode pattern, changing the poling and stress direction, layering the material to maximize the active volume, adding pre-stress to maximize the coupling and applied strain of the material, and tuning the resonant frequency of the device.

The type of piezoelectric material selected for a power harvesting application can have a major influence on the harvester's functionality and performance. Although PZT is widely used as a power harvesting material, the piezoceramic's extremely brittle nature causes limitations in the strain that it can safely absorb without being damaged. It is however the most easily available transducer material.

II. MODELING OF PIEZOELECTRICITY ON BEAMS AND PLATES

Some previous works done on the mathematical modeling of piezoelectric energy harvesting utilized simple single degree of freedom lumped parameter modeling approaches (Stephen, 2006), (Dutoit, et al., 2005). There has been an attempt to improve on this which has led to the investigation of the distributed parameter models utilizing the Rayleigh-Ritz discretization, which gives more accurate solutions (Dutoit, et al., 2005), (duToit & Wardle, 2007), (Sodano & Inman, 2004). There have also been efforts to develop exact analytical solutions of the piezoelectric cantilever harvester based on Euler-Bernoulli beam theory (Ajitsaria, et al., 2007), (Chen, et al., 2006).

Exact solutions were provided for symmetric bimorph piezoelectric cantilever energy harvesters (Erturk & Inman, 2009) although many practical piezoelectric harvester configurations are more complicated. The simplest energy harvesting circuit is the full wave rectifier (to convert the AC signal to all positive voltage) combined with a smoothing capacitor (to convert the signal to DC).

The defining equations for high permittivity dielectrics are

$$C = \frac{K\varepsilon_r A}{t} = \frac{\varepsilon_o \varepsilon_r A}{t} = \frac{\varepsilon A}{t} \quad (1)$$

And

$$Q = CV = \frac{\varepsilon AV}{t} \quad (2)$$

where,
C = capacitance
A = capacitor plate area (m^2)
ε_r = relative dielectric constant
ε_o = dielectric constant of air = 8.85×10^{-12} faradays/ meter
ε = dielectric constant
V = voltage
t = thickness or plate separation
Q = charge

In addition, electric displacement D, which can be defined as the charge density or the ratio of charge to the area of the capacitor can be expressed as:

$$D = \frac{Q}{A} = \frac{\varepsilon V}{t} \quad (3)$$

The electric field can also be expressed as:

$$H = \frac{V}{t} \quad (4)$$

These equations hold true for all isotropic dielectrics and there is a direct relationship between the ratio of dielectric displacement, D, and the electric field, H.

Hence,

$$D = \varepsilon H \quad (5)$$

2.1 Coupling

Coupling helps in evaluating the quality of an electro-mechanical material and represents the efficiency of the conversion of energy from electrical to mechanical or vice-versa

$$K_1 = \frac{Mechanical\ energy\ converted\ to\ electrical\ charge}{Mechanical\ energy\ input} \quad (6)$$

or

$$K_2 = \frac{Electrical\ energy\ converted\ to\ mechanical\ displacement}{Electrical\ energy\ input} \quad (7)$$

where K_2 stands for the constant.

The piezoelectric effect can be described using the coupled equations (D. Damjanovic, 1998) (Meitzler, et al., 1998)

$$S = s^E.T + d^t.E \quad (8)$$
$$D = d\,.T + \varepsilon^T\,.E \quad (9)$$

where S is the mechanical strain [m/m], T is the mechanical stress [N/m^2], D is the electrical displacement [C/m^2] (charge density), E is the electric field [N/C or V/m], s^E is the compliance under a zero or constant electrical field indicated by the superscript E and ε^T is the dielectric permittivity under a zero or constant stress [F/m] indicated by the superscript T while d and d^t are the matrices for the direct and the reverse piezoelectric effect, where the superscript t means the transposed matrix. Thus, Equations (8) and (9) describe the reverse and the direct piezoelectric effect, respectively. Without the coupling term $d^t.E$, (8) is simply Hooke's law relating strain and stress. Likewise, Equation (9) is the dielectric equation when the coupling term $d \cdot T$ is neglected. The detailed matrix notation of Equations (8) and (9) for a material of the 6 mm crystal class such as PZT ceramic is shown in Equations (10) and (11):

2.2 Piezoelectric Coefficients and Terminology

Piezoelectric materials are characterized by several coefficients that link electrical and mechanical quantities in what is termed the "d" coefficients. They are represented by subscripts designating the directions of the electrical and mechanical quantities that are directly linked to the coordinate system.

Figure 3 presents an example of this, the point is that the first subscript always refers to the direction of electric field (applied or induced), and the second always refers to direction of stress (applied or induced).

The "d" constant has many names, it is referred to as the strain constant, charge constant, the piezo modulus etc. It is commonly expressed in terms of coulombs/newton. It should be noted that this expresses the "d" coefficient in transducer mode, which means it goes from mechanical to electrical energy, i.e., how many coulombs we get for each newton applied.

Through application of dimensional analysis, the "d" coefficient can be expressed as strain divided by applied electric field which can be further simplified to meters per volt, and is a measure of how much the material changes in length in response to applied voltage.

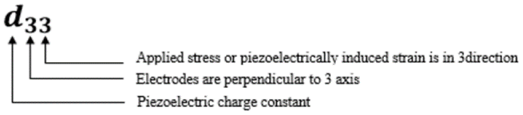

Figure 3: Piezoelectric constant and terminology

2.3 Axis Nomenclature

Piezoelectric effects, are highly dependent upon the orientation of the poled axis. It is, therefore, essential to maintain a constant axis numbering scheme. This is shown in Figure 4

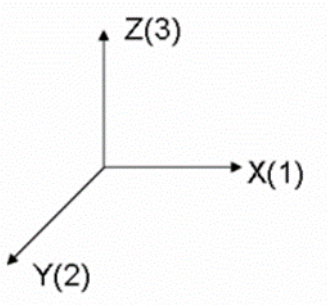

Figure 4: Axis nomenclature

For electromechanical constants:

d_{ab}, a = electrical direction; b = mechanical direction

$$\begin{bmatrix} S_1 \\ S_2 \\ S_3 \\ S_4 \\ S_5 \\ S_6 \end{bmatrix} = \begin{bmatrix} s_{11}^E & s_{12}^E & s_{13}^E & 0 & 0 & 0 \\ s_{12}^E & s_{11}^E & s_{13}^E & 0 & 0 & 0 \\ s_{13}^E & s_{13}^E & s_{33}^E & 0 & 0 & 0 \\ 0 & 0 & 0 & s_{44}^E & 0 & 0 \\ 0 & 0 & 0 & 0 & s_{11}^E & 0 \\ 0 & 0 & 0 & 0 & 0 & 2(s_{11}^E - s_{12}^E) \end{bmatrix} \begin{bmatrix} T_1 \\ T_2 \\ T_3 \\ T_4 \\ T_5 \\ T_6 \end{bmatrix} + \begin{bmatrix} 0 & 0 & d_{31} \\ 0 & 0 & d_{31} \\ 0 & 0 & d_{31} \\ 0 & d_{31} & 1 \\ d_{31} & 0 & 0 \\ 0 & 0 & 0 \end{bmatrix} \begin{bmatrix} E_1 \\ E_2 \\ E_3 \end{bmatrix} \quad (10)$$

$$\begin{bmatrix} E_1 \\ E_2 \\ E_3 \end{bmatrix} = \begin{bmatrix} 0 & 0 & 0 & 0 & d_{15} & 0 \\ 0 & 0 & 0 & d_{15} & 0 & 0 \\ d_{31} & d_{31} & d_{33} & 0 & 0 & 0 \end{bmatrix} \begin{bmatrix} T_1 \\ T_2 \\ T_3 \\ T_4 \\ T_5 \\ T_6 \end{bmatrix} + \begin{bmatrix} \varepsilon_{11}^T & 0 & 0 \\ 0 & \varepsilon_{11}^T & 0 \\ 0 & 0 & \varepsilon_{33}^T \end{bmatrix} \begin{bmatrix} E_1 \\ E_2 \\ E_3 \end{bmatrix} \quad (11)$$

The subscripts 1, 2 and, 3 are related to the *x*, *y*, *z* axes in the Cartesian coordinate system. Due to symmetrical reasons, many matrix elements are zero, and only a few are independent. Generally, *D* and *E* are vectors, i.e., tensors of rank 1, and the permittivity is a tensor of rank 2. In principle, strain *S* and stress *T* are also tensors of rank 2, but due to the symmetry of the strain and stress tensors, the subscripts are conventionally re-labeled according to the so-called Voigt notation (Meitzler, et al., 1998): 11 → 1; 22 → 2; 33 → 3; 23 → 4; 13 → 5; 12 → 6. Thus, they can be written as vectors or rank-1 tensors in Equations (10) and (11). Due to the Voigt notation, the order of the compliance tensor can be reduced from 4 to 2, resulting in the 6 × 6 matrix in Equation (10)

2.4 Harvester Modes of Operation

Assuming a beam of piezoelectric material, as displayed in Figure 5, one might notice there are several ways of utilizing the piezo effect for energy harvesting, depending on where the mechanical energy is applied and where the electrodes are connected.

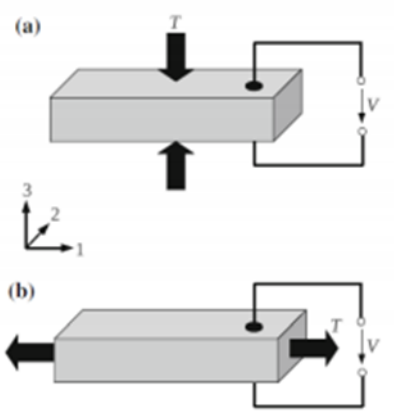

Figure 5: Piezoelectric material operated in (a) 33 and (b) 31 mode (Hehn & Manoli, 2015)

In Figure 5 a) we can see a block of material in the 33 modes, because a stress T acts in the same direction as the poling. The device actuation direction is in the 33-direction that is force and poling directions are same and so a better performance can be obtained from the actuator depending on the number of the piezoelectric layers making the piezoelectric stack actuator the most common force-generating device. In Figure 5 b) the 31 mode is displayed, since the stress is parallel to the beam, this is the most commonly used mode for energy harvesters. Generally, cantilever beams are the 31-types in which the configuration is such that the poling direction is perpendicular to the stress direction and electrodes cover the whole top and bottom surface of the piezoelectric layer.

2.4 Types of Piezoelectric Materials

There are many kinds of piezoelectric materials that can be used to harvest ambient vibration energy but the main classes are: piezoelectric materials ceramics, crystals that have a natural piezoelectricity, macro fiber composite (MFC), polymers and polarized composites. In terms of the performance of different material on Piezoelectric Energy Harvesting. Ferroelectric lead zirconate titanate is most frequently used piezoelectric ceramic for sensor applications due to its superior electromechanical coupling factor (Ivan, et al., 2010). A number of lead-free ferroelectric and piezoelectric materials have been recently explored (Aksel & Jones, 2010).

Table 1 shows the properties of these materials. In general, the piezoelectric material is coupled to a resonant structure which imposes a strain or vibration. Due to piezoelectricity, this deformation is converted into electrical charge by different means which are compressed, slap and bending.

Table 1: Some properties of common piezoelectric materials (Beeby, et al., 2006)

Material	$BaTiO_3$	PZT 5A	PZT 5H	PVDF
d_{31} $(\times 10^{-12}\mathrm{CN}^{-1})$	78	-171	-274	23
d_{33} $(\times 10^{-12}\mathrm{CN}^{-1})$	149	374	593	-33
g_{31} $(\times 10^{-3}\mathrm{VmN}^{-1}$	5	-11.4	-9.1	216
g_{33} $(\times 10^{-3}\mathrm{VmN}^{-1}$	14.1	24.8	19.7	330
k_{31}	0.21	0.31	0.39	0.12
k_{33}	0.48	0.71	0.75	0.15
Relative permittivity ($\varepsilon/\varepsilon 0$)	1700	1700	3400	12
Young's modulus (GPa)	67	50	50	2

There are many different methods of modeling piezoelements. Among them are as listed:

- Equivalent circuit,
- Spring model,
- Thermal analogy,
- Finite element method.

In this work, the finite element method (FEM) was used to model the various cantilever beam.

COMSOL Multiphysics software was used to develop a finite element model of the piezoelectric energy harvester cantilever beam. It provides an Interdigitated Electode (IDE) and unified workflow for mechanical, fluid, electrical and chemical applications and the Microelectromechanical System (MEMS) Module which provides predefined user interfaces with a variety of coupled physics, including electromagnetic-

structure, thermal-structure or fluid-structure interactions. The Structural Mechanics module is useful in the analysis of mechanical structures that are subjected to static or dynamic loads. It can be used for a wide range of analysis types, including stationary, transient, eigenmode/modal, parametric, quasi-static, frequency response, buckling and pre-stressed. (N.Siddaiah, et al., 2017).

The materials used in the simulation are:

- Piezoelectric materials: PDVF, PZT4, PZT 5A, ZnO
- Substrate's materials: Aluminum, Silicon and Titanium Beta-21S.

III. MATHEMATICAL MODELING OF PIEZOELECTRIC ENERGY HARVESTING

There are various assumptions made throughout the simulation of these beams. Some of these assumptions are made purely for the sake of these simulations and others are more universal assumptions for the beam theory.

3.1 Assumptions for Simulation

- There are no external forces or moments other than those inputted by the user and those anchoring the beams
- The anchored end of the beam remains completely unmoved
- During static analysis all inputs are held constant
- On the micro scale gravitational forces are miniscule relative to electric forces
- The beam has a rectangular cross section.

3.2 Beam Theory

The Euler-Bernoulli Beam equation is used in analyzing the deflection and characteristics of beams when load is applied. The assumptions made in applying this equation include:

- Continuum mechanics is valid for a bending beam.
- The stress at a cross section varies linearly in the direction of bending, and is zero at the center of every cross section.
- The bending moment at a particular cross section varies linearly with the second derivative of the deflected shape at that location.
- The beam is composed of an isotropic material.
- The applied load is orthogonal to the beam's neutral axis and acts in a unique plane.

The linear constitutive equations for a piezoelectric material (Seuaciuc-Osorio & Daqaq, 2010) have been employed in terms of the piezoelectric coefficient e_{31}, the dielectric constant ε_{33} and the electric field applied across the thickness of the layer E_z. Hence,

$$D = e_{31}\varepsilon_x + \varepsilon_{33}E_z \qquad (12)$$

The stress σ in z-direction is assumed zero. This occurs when piezoelectric layer thickness in comparison to the length of the beam can be considered very thin.

3.3 The Cantilever Beam Model

Figure 6 shows the setup for the cantilever beam model. Following the Euler Bernoulli definition of a beam, the length is over ten times larger than the width. The PZT is attached to the beam near the clamped edge for maximum strain. For the estimated power that a PZT can produce from beam vibrations to be calculated, the moment that the PZT experiences must first be determined. This moment can be evaluated by solving for the deflection of the beam and then estimating the experienced moment as a function of the beam's curvature.

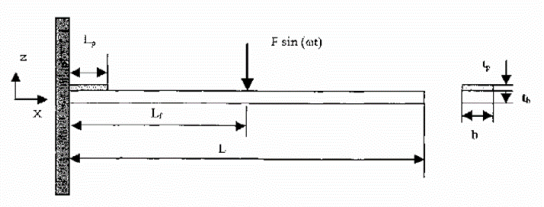

Figure 6: cantilever beam model

The Euler-Bernoulli method is used to model the cantilever beam. The governing un-damped equation of motion for the beam for forced motion under zero initial conditions can be written as:

$$\rho A \frac{\partial^2 w(x,t)}{\partial t^2} + E_b I_b \frac{\partial^4 w(x,t)}{\partial x^4} = F(t) \qquad (13)$$

where w is the displacement of the beam, ρ is the density of the steel beam, A is the cross-sectional area, and $F(t)$ is the external force applied to the beam. The boundary conditions are:

$$w(0,t) = 0,$$

$$w_x(0,t) = 0,$$
$$w_{xx}(L_b,t) = 0,$$
$$w_{xxx}(L_b,t) = 0,$$

Considering a harmonic forcing function applied to a single point on the beam, according to Figure 6, we can write:

$$\frac{\partial^2 w(x,t)}{\partial t^2} + c^2 \frac{\partial^4 w(x,t)}{\partial x^4} = \frac{F_0}{\rho A}\sin(\omega t)\,\delta\left(x - L_f\right) \quad (14)$$

where ω is the frequency, L_f is the position of the applied force and c2 can be written as:

$$c^2 = \frac{E_b I_b}{\rho A} \quad (15)$$

The frequency will be equal to the beam's first natural frequency because the largest deflections occur at the first natural frequency. A general solution for this equation is given by:

$$w(x,t) = \sum_{i=1}^{3} q_i(t)\mathrm{X}_i(x) \quad (16)$$

where q_i is the *i-th* modal coordinate equation of the beam and X_i is the *i-th* mode shape of the beam. For consistency, only the first three mode shapes will be used in the summation process described by Equation (16). Therefore, considering the free un-damped vibration,

$$\mathrm{X}_i(x)\frac{\partial^2 q_i(t)}{\partial t^2} = -c^2 \frac{\partial^4 \mathrm{X}_i(x)}{\partial x^4} q(t) \quad (17)$$

Using the standard method of separation of variables in the solution of Equation (17), we have the equations:

$$-\frac{\frac{\partial^2 q_i(t)}{\partial t^2}}{q(t)} = \frac{c^2 \frac{\partial^4 \mathrm{X}_i(x)}{\partial x^4}}{\mathrm{X}_i(x)} = {\omega_n}^2 \quad (18)$$

Here, we can write the Equation (18) as:

$$\begin{cases} \frac{\partial^2 q_i(t)}{\partial t^2} + {\omega_n}^2 q_i(t) = 0 \\ \frac{\partial^4 \mathrm{X}_i(x)}{\partial x^4} - \frac{{\omega_n}^2}{c^2}\mathrm{X}_i(x) = 0 \end{cases} \quad (19)$$

The solution of the second equation in Equation (19) is:

$$\mathrm{X}_i(x) = A_1\cos(\beta_i x) + A_2\sin(\beta_i x) + A_3\cosh(\beta_i x) + A_3\sinh(\beta_i x) \quad (20)$$

Applying the boundary conditions is found the general mode shape equation for a cantilever beam

$$\beta_i = \sqrt{\frac{{\omega_{ni}}^2}{c^2}} \quad (21)$$

Where L_b is the beam length. In the Eq. (3.10), $i\_$ can be written as:

$$\cos(\beta_i L_b)\cosh(\beta_i L_b) = -1 \quad (22)$$

More details regarding the solution process can be found in Inman (Poulin, et al., 2004)
For the first equation in Equation (19), we have the solution:

$$q_i(t) = \frac{1}{\omega_{di}} e^{-\zeta\omega_{ni}t}\int_0^t F_i(\tau)\, e^{-\zeta\omega_{ni}t}\sin\left(\omega_{di}(t-\tau)\right) d\tau \quad (23)$$

where ω_{ni} is the damped natural frequency and ζ is the damping ratio.

3.4 Energy Harvesting Configuration

Cantilever beam consists of two layers, base layer (silicon, Aluminum, Titanium beta 21S) and upper layer made up of piezoelectric material (PVDF, PZT 4, PZT 5A, Zinc Oxide). The one end of the beam is fixed and another end is suspended freely. The mechanical energy of the beam gets converted into electrical energy by the process shown in Figure 7.

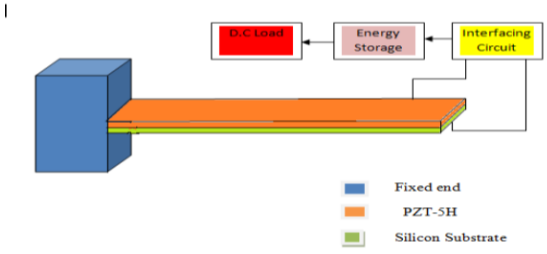

Figure 7: Model of energy harvesting system

The interfacing circuit includes a transducer to convert mechanical energy produced as a result of deflection from cantilever beam to electric power and also consists of harvesting circuit which is used to optimize

the harvesting efficiency (Cook-Chennault, et al., 2008). The flow chart in Figure 8 below describes the steps involved in the designing of cantilever geometry

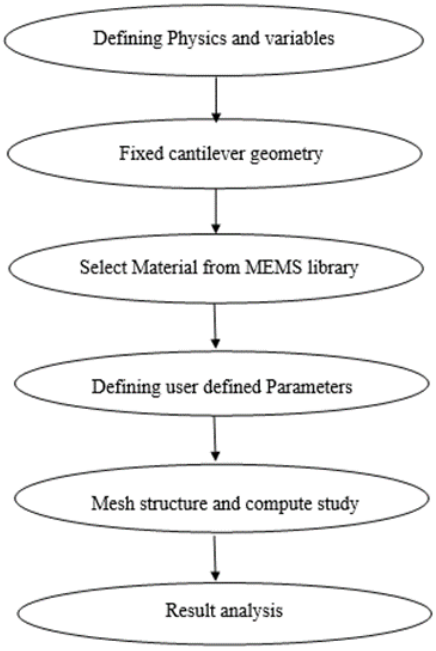

Figure 8: Modeling Process steps for energy harvesting

3.5 Design Parameters

3.5.1 Geometry

The U-shaped and E-shaped cantilever was designed and compared with the rectangular cantilever beam to determine which geometry would give the optimal output power.

One of the cantilever ends is assigned a fixed boundary condition and the other ends are given free boundary conditions. The bottom of the piezoelectric layer as ground and assign a floating potential condition to the top surface of the piezoelectric layer. A constant force of 10N is applied on all the cantilevers.

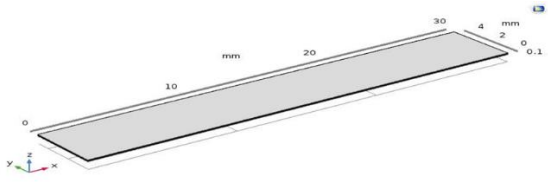

Figure 9: Designed model of rectangular cantilever beam in COMSOL

Table 2: Geometry properties of a rectangular cantilever beam

Symbol	Description	Value(mm)
L_b	Beam Length	30
W_b	Beam Width	5
t_p	Thickness of piezoelectric material	0.06
t_s	Thickness of substrate material	0.04

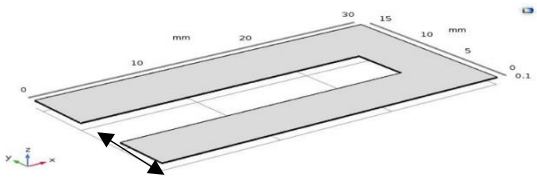

Element Spacing

Figure 10: Designed model of U-shaped cantilever beam in COMSOL

Table 3: Geometry properties of a U-shaped cantilever beam

Symbol	Description	Value(mm)
L_b	Beam Length	30
W_b	Beam Width	15
t_p	Thickness of piezoelectric material	0.06
t_s	Thickness of substrate material	0.04
	Element Spacing	5

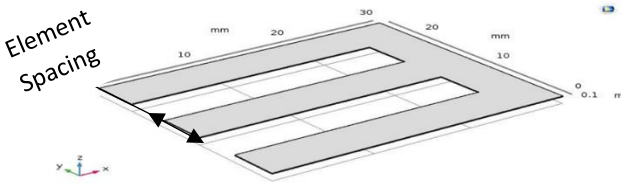

Figure11: Designed model of E-shaped cantilever beam in COMSOL

Table 4: Geometry properties of a E-shaped cantilever beam

Symbol	Description	Value(mm)
L_b	Beam Length	30
W_b	Beam Width	25

t_p	Thickness of piezoelectric material	0.06
t_s	Thickness of substrate material	0.04
	Element Spacing	5

The deflection of the cantilever beam depends up on the dimensions of the beam i.e., length, width, thickness and also depends on various properties of the material used to build the cantilever.

The following equation relates cantilever end deflection 'δ' to applied stress 'σ'.

$$\delta = \frac{3\sigma(1-\nu)}{Y}\frac{{L_b}^2}{t^2} \quad (24)$$

Where 'ν' is Poisson's ratio, 'Y' is Young's modulus, 'L_b' is the beam length and 't' is the cantilever thickness. The cantilever spring constant 'k' relates to the cantilever dimensions and material constants are given by:

$$k = \frac{F}{\delta} = \frac{YW_b t^3}{4{L_b}^3 k} \quad (25)$$

Where 'F' is the applied force and 'δ' is the applied stress, Y is young modulus, 't' is the thickness of the cantilever beam, 'L_b' is the total length, 'W_b' is the width and 'k' is the rotational stiffness. The movement of the cantilever is effected by its length, depth, thickness and various properties of the material used to make the structure. The geometric shape, as well as the material used to build the cantilever determines the cantilever's stiffness. Thus the sensitivity of the cantilever beam changes with the change is shape of the cantilever.

The power is calculated from equation 3.3

$$P_{ave} = \frac{V^2}{R_{load}} \quad (26)$$

Where 'P_{ave}' is the average power generated and 'V' is the electric potential found via the simulation of the cantilever beams and R_{load} is the resistive load or impedance (Shen D, et al., 2008).

3.6 Material Properties

Table 5: Properties of Substrate Materials

Material	Description	Unit
Aluminum	Density	2700 kg/ m^3
	Young's Modulus	70GPa
	Poisson ratio	0.33
Silicon	Density	2329 kg/ m^3
	Young's Modulus	170GPa
	Poisson ratio	0.28
Titanium beta-21S	Density	4940kg/ m^3
	Young's Modulus	105GPa
	Poisson ratio	0.33

Table 6: Properties of the Piezoelectric Materials

Material	Description	Unit
PVDF	Density	1780kg/ m^3
	Young's Modulus	GPa
	Poisson ratio	0.34
PZT 4	Density	7500kg/ m^3
	Young's Modulus	62GPa
	Poisson ratio	0.35
PZT 5A	Density	7750kg/ m^3
	Young's Modulus	50GPa
	Poisson ratio	0.35
ZnO	Density	5680kg/ m^3
	Young's Modulus	GPa
	Poisson ratio	0.33

3.7 Meshing

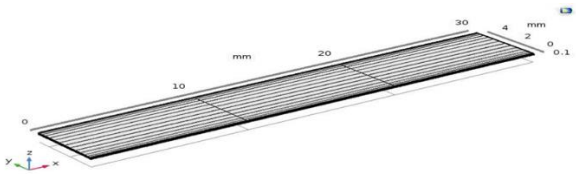

Figure 12: Meshed Model of a Rectangular Cantilever beam

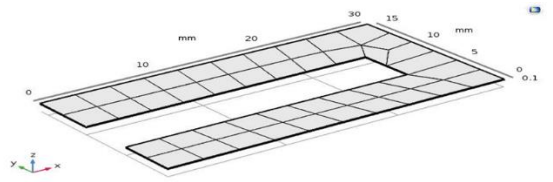

Figure 13: Meshed Model of a U-shaped cantilever beam

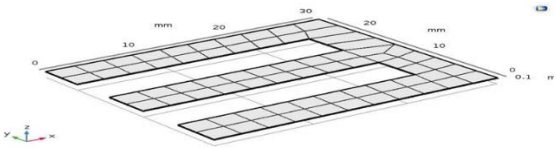

Figure 14: Meshed model of an E-shaped cantilever beam

IV. RESULTS AND DISCUSSION

Figures (15) to (20), depict the displacement and generated piezoelectric voltages for various geometries simulated and different piezoelectric material. As per theoretical criteria, it was observed that there was an increase in deflection with a decrease and hike in electric potential which leads to the increase in the generated power as also noted in literature (V.M & G.V, 2013)

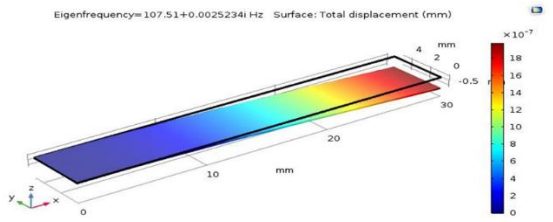

Figure 15: Deformed shape of the rectangular shaped beam when a 10N force is applied

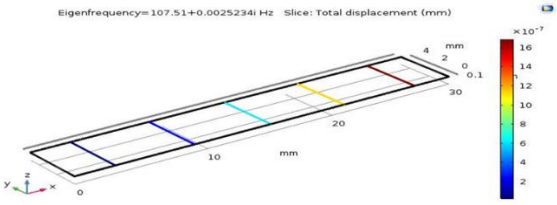

Figure 16: Cantilever beam electric potential

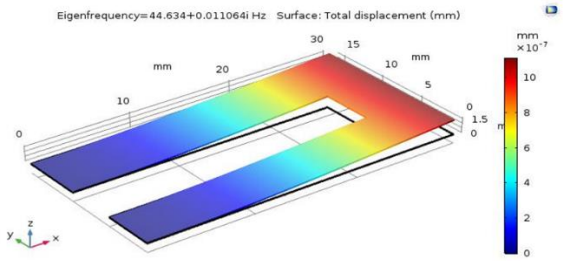

Figure 17: Deformed shape of the U-shaped beam when a 10N force is applied

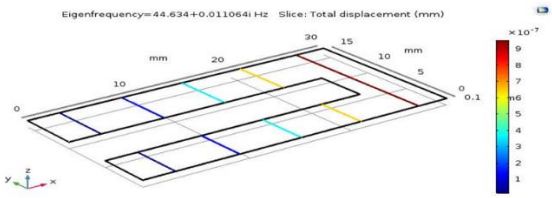

Figure 18: Cantilever beam electric potential

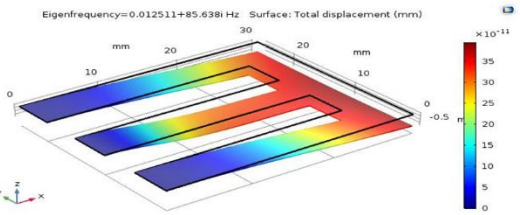

Figure 19: Deformed shape of the E-shaped beam when a 10N force is applied

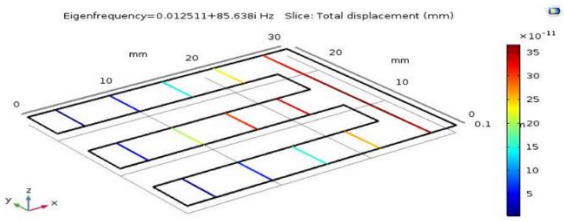

Figure 20: Cantilever beam electric potential

- Performance based on length and width of various shaped cantilever beam

The variation of frequency with length and width of beam are in Figure shown below. Figure 4.7 depicts that as the rectangular cantilever beam length increases, the frequency decreases when the width and thickness is fixed at 5mm and 0.16mm. Figure 4.8 shows that the frequency slowly increases with the width of the beam.

Figure 4.7, 4.8 shows the same variation as figure 4.9, 4.10, that is; frequency decreases with beam length and slowly increases with the width of the beam.

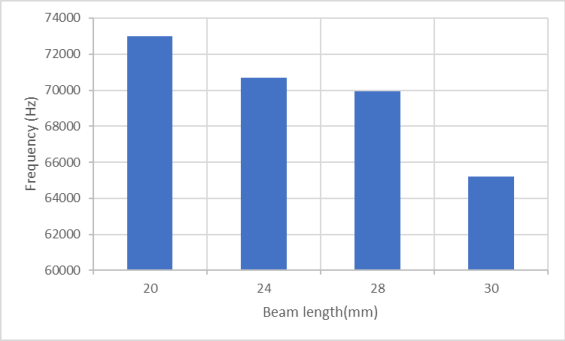

Figure 21: Variation of frequency with the length of the beam for a rectangular cantilever

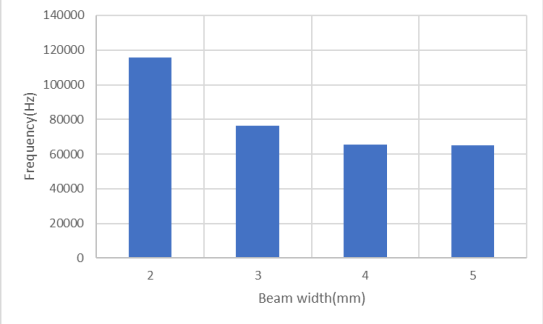

Figure 22: Variation of frequency with the width of the beam for a rectangular cantilever

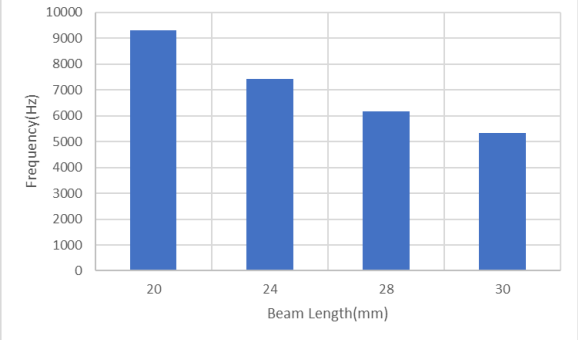

Figure 23: Variation of frequency with the length of the beam for a U-shaped cantilever

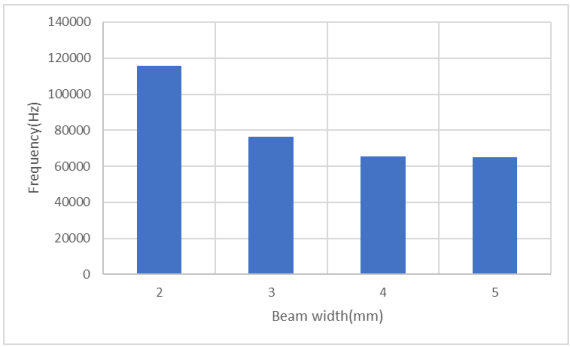

Figure 24: Variation of frequency with the width of the beam for a U-shaped cantilever

CONCLUSION

In this work, piezoelectric cantilever energy harvester with different materials of varying dimensions and shapes were studied. The simulations were carried out to predict the output voltage (V) across the piezoelectric layers for different piezoelectric materials and substrate materials with various shaped cantilever beam. A rectangular beam with dimension 30 mm x 5 mm x 0.16 mm, and a U-shaped beam with dimension 30 mm x 15 mm x 0.16mm in addition to an E-shaped beam with dimension 30 mm x 25 mm x 0.16 mm were examined. COMSOL Multiphysics 5.3 was used for simulation. The properties examined included; variation of the beam length and beam width with respect to frequency. Also, the variation of eigen frequency with voltage was examined for the different cantilever structures. All the cantilever structures were studied at resonance frequency between 60 to 200Hz. It was observed that the E-shaped structure gave a maximum voltage of 8.792V at the eigen frequency of 0.032Hz with applied force of 10N. The PZT 5A with Aluminum substrate demonstrates best performance in context of voltage output and eigen frequency compared to other piezoelectric materials under study. For energy harvesting the E-shaped cantilever structure using PZT-5A as piezoelectric layer and Aluminum as a substrate layer gave the best result.

REFERENCES

[1] Abrol, S. & Chhabra, D., (2017). Harvesting Piezoelectricity using Different Structures by Utilizing Fluid Flow. INTERNATIONAL JOURNAL OF R&D IN ENGINEERING,

SCIENCE AND MANAGEMENT, 5(7), pp. 24-36.

[2] Ajitsaria, J., S. Y. C., D. S. & Kim, D. J., (2007). Modeling and analysis of a bimorph piezoelectric cantilever beam for voltage generation. Smart Materials and Structures, 16(2), pp. 447-454.

[3] A, K. M., R, F. J. & J, I. D., (2013). Parametrically excited nonlinear piezoelectric compact wind turbine. Renewable Energy, pp. 977-987.

[4] Aksel, E. & Jones, J. L., (2010). Advances in lead-free piezoelectric materials for sensors and actuators. Sensors, 10(3), pp. 1935-1954.

[5] Anton, S. R., Erturk, A. & Inman, D. J., (2009). Piezoelectric energy harvesting from multifunctional wing spars for UAVs – Part 2: experiments and storage applications. Active and Passive Smart Structures and integrated systems, Volume 7288, pp. 1-12.

[6] Anton, S. R. & Sodano, H. A., (2007). review of power harvesting using piezoelectric materials (2003-2006). Smart Materials and Structures, Volume xvi, pp. 1-21.

[7] Beeby, S. P., Tudor, M. J. & White, N. M., (2006). Energy harvesting vibration sources for microsystems applications. Measurement Science and Technology, Volume 17, pp. 175-195.

[8] Chen, S.-N., Wang, G.-J. & Chien, M.-C., (2006). Analytical modeling of piezoelectric vibration-induced micro power generator. Mechatronics, 16(7), pp. 379-387.

[9] C, M. T. T. & N, S. G., (2010). Use of a piezo-composite generating element for harvesting wind energy in an urban region. Aircraft Engineering and Aerospace Technology , 82(6), pp. 376-381.

[10] Cook-Chennault, K. A., N, T. & M, S. A., (2008). Powering MEMS portable devices-a review of non-regenerative and regenerative power supply systems with special emphasis on piezoelectric energy harvesting systems. Smart Materials and Structure, Volume 4, p. 17.

[11] Datta. S., (2014). Piezoelectric Materials: Crystal Orientation and Poling Direction. Available: https://www.comsol.com/blogs/piezoelectric-materials-crystal-orientationpoling-directio

[12] duToit, N. E. & Wardle, B. L., (2007). Experimental Verification of Models for Microfabricated Piezoelectric Vibration Energy Harvesters. AIAA Journal, 45(5), pp. 1126-1137.

[13] Dutoit, N. E., Wardle, B. L. & Kim, S.-G., (2005). Design considerations for MEMS-scale piezoelectric mechanical vibration energy harvesters. Integrated Ferroelectrics, 71(1), pp. 121-160.

[14] Elvin, N. G. & Elvin, A. A., (2009). A General Equivalent Circuit Model for Piezoelectric Generators. ournal of Intelligent Material Systems and Structures, 20(1), pp. 3-9.

[15] Erturk, A., (2012). Assumed-modes formulation of piezoelectric energy harvesters: Euler–Bernoulli,Rayleigh, and Timoshenko models with axial deformations. Computers and Structures, Volume 106-107, pp. 214-227.

[16] Erturk, A. & Inman, D. J., (2008). Issues in mathematical modeling of piezoelectric energy harvesters. Smart Materials and Structures, 17(6), pp. 2-15.

[17] Erturk, A. & Inman, D. J., (2008). On Mechanical Modeling of Cantilevered Piezoelectric Vibration Energy Harvesters. Journal of Intelligent Material Systems and Structures, Volume 19, pp. 1-15.

[18] Erturk, A. & Inman, D. J., (2009). An experimentally validated bimorph cantilever model for piezoelectric energy harvesting from base excitations. Smart Materials and Structures, 18(025009), pp. 1-18.

[19] G.E, B., M, D. V. & S, D. A., (2017). Fluids energy harvesting system with low cut-in velocity piezoelectric MEMS. IEEE International Conference on IC Design and Technology, pp. 1-4.

[20] Gao, X. et al., (2018). Giant Piezoelectric Coefficients in Relaxor Piezoelectric Ceramic PNN-PZT for Vibration Energy Harvesting. Advance Functional Materials, Issue 10, pp. 1-8.

[21] German Martinez-Ayuso, M. I. F. S. A. H. K. H. B.,(2017). Homogenization of porous piezoelectric materials. Solid and Structures, pp. 1-26.

[22] Harstad, S. et al., (2017). Enhancement of β phase in PVDF films embedded with ferromagnetic Gd5Si4 nanoparticles for piezoelectric energy harvesting. American Institue of Physics Advances, pp. 1-8.

[23] Hehn, T. & Y. Manoli, (2015). CMOS Circuits for Piezoelectric Energy Harvesters.

[24] Hwang, G.-T.et al., (2015). A Reconfi gurable Rectifi ed Flexible Energy Harvester via Solid-State Single Crystal Grown PMN–PZT. Advanced Energry materials, pp. 1-8.

[25] Isarakorn, D. et al., (2010). Epitaxial piezoelectric MEMS on silicon. Journal of Micromechanics and Microengineering, x(20), pp. 1-10.

[26] Ivan, L. A., Rakotondrabe, M. & Agnus, J., (2010). Comparative material study between PZT ceramic and newer crystalline PMN-PT. Reviews on Advanced Materials Science, 24(1-2), pp. 1-9.

[27] J. I. Roscow, J. T. &. C. R. B., (2016). Manufacture and characterization of porous ferroelectrics for piezoelectric energy harvesting applications. Ferroelectrics, Volume 498, pp. 40-46.

[28] J, E. A. a. I. D., (2008). A Distributed Parameter Electromechanical Model for Cantilevered Piezoelectric Energy Harvesters. Journal of Vibration and Acoustics, 130(041002), pp. 1-15.

[29] Kishore, R. A., Vučković, D. & Priya, S., (2014). Ultra-Low Wind Speed Piezoelectric windmill. Ferroelectrics, Volume 10, pp. 1-11.

[30] K, U., (2017). The development of piezoelectric materials. In: Advanced Piezoelectric Materials. Amsterdam: Elsevier, pp. 1-92.

[31] .Lee, S. W. et al.,(2014). An electrochemical system for efficiently harvesting low-grade heat energy. NATURE COMMUNICATIONS, Volume 5.

[32] Lefeuvre, E., Audigier, D., Richard, C. & Guyomar, D., (2007). Buck-Boost Converter for Sensorless Power Optimization of Piezoelectric Energy Harvester. IEEE Transactions on Power Electronics, 22(5), pp. 1-9..

[33] Meitzler, A.H. H.F. Tiersten, A.W. Warner, D. Berlincourt, G.A. Couqin, F.S. Welsh III, IEEE Standard on Piezoelectricity. Institute of Electrical and Elec- tronics Engineers (IEEE), New York (1988)

[34] Messing, G. L. et al., (2004). Templated Grain Growth of Textured Piezoelectric Ceramics. Critical Reviews in Solid State and Materials Sciences, 2(29), pp. 45-96.

[35] Myers, R., Vickers, M., Kim, H. & Priya, S., (2007). Small scale windmill. Applied Physics Letters, Volume 90, pp. 1-4.

[36] N.Siddaiah, et al., (2017). DESIGN AND MODEL ANALYSIS OF VARIOUS SHAPE CANTILEVER. Journal of Advanced Research in Dynamical and Control Systems, Volume 9.

[37] P. Muralt, R. P. a. S. T.-M., (2009). Piezoelectric Thin Films for Sensors, Actuators, and Energy Harvesting. MRS BULLETIN, Volume 34, pp. 1-7.

[38] Palneedi, H. et al., (2017). Strong and anisotropic magnetoelectricity in composites ofmagnetostrictive Ni and solid-state grown lead-free piezoelectricBZT–BCT single crystals. Journal of Asian Ceramic Societies, pp. 1-6.

[39] Pan, C. et al., (2015). Significant Piezoelectric and Energy Harvesting Enhancement of Poly(vinylidene fluoride)/Polypeptide Fiber Composites Prepared Through Near-Field Electrospinning. Materials Chemistry A, pp. 1-9.

[40] Poulin, G., Sarraute, E. & Costa, F., (2004). Comparative study of an electromagnetic and a piezoelectric system, Sensors and Actuators A. Generation of electrical energy for portable devices, Issue 116, pp. 461-471.

[41] Priya, S., (2005). Modeling of electric energy harvesting using piezoelectric windmill. Applied Physics Letters, Volume 87, pp. 1-4.

[42] Priya, S., Chen, C.-T., Fye, D. & Zahnd, J., (2004). Piezoelectric Windmill: A Novel Solution to Remote Sensing. Japanese Journal of Applied Physics, Volume 44, pp. 1-7.

[43] Rao, G. B., Rajesh, P. & Ramasamy, P., (2016). Investigations on the growth, optical, thermal, dielectric, and laser damage threshold properties of crystal violet dye-doped potassium acid phthalate single crystal. Applied physics A Materials Science and processing, pp. 1-9.

[44] Richard, Y. L. a. C., (2014). Piezogenerator impedance matching using Mason equivalent circuit for harvester identification in Proc. SPIE 9057, Active and Passive Smart. San Diego, California, s.n.

[45] Seema A, K. R. D., Varghese & M., a. J., (2007). "PVDF-PZT-5H composites prepared by hot press and tape casting techniques.. Journal of applied polymer science, 106(1), pp. 146-151.

[46] Seuaciuc-Osorio, T. & Daqaq, M. F., (2010). Energy harvesting under excitations of time-varying frequency. Journal of Sound and Vibration, Issue 329, pp. 249-251.
[47] Shahab, S., Zhao, S. & Erturk, A., (2018) Performance Comparison of Soft and Hard Piezoelectric Ceramics and Single Crystals for Random Vibration Energy Harvesting. Energy Technology, pp. 1-9.
[48] Shen D, J. P., J, A., Choe SY, W. H. & DJ, K., (2008). J Micromech Microeng. The design, fabrication and evaluation of a MEMS PZT cantilever with an integrated Si proofmass for vibration energy harvesting, p. 18.
[49] Sodano, H. A. & Inman, D. J., (2004). Estimation of Electric Charge output for Piezoelectric Energy Harvesting. Strain Journal, 40(2), pp. 49-58.
[50] Stephen, N., (2006). On energy harvesting from ambient vibration. Journal of Sound and Vibration, Volume 293, pp. 409-425.
[51] Tabesh, A. & Fréchette, d. L. G., (2010). Low-Power Stand-alone Adaptive Circuit for Micropower Generator. IEEE Transactions on Industrial Electronic, 57(3), pp. 1-10.
[52] V.M, R. & G.V, S., (2013). design and analysis of microcantilevers with various shapes. International Journal of Emerging and Advance Engineering, Volume III.
[53] Vullers, R. et al., (2014). Smart Sensor Systems. In: Micropower Generation: Principles and Applications. s.l.:John Wiley & Sons Ltd, pp. 237-274.
[54] Wang, X., (2012). Piezoelectric nanogenerators - Harvesting ambient mechanical energy at the nanometer scale. Nano Energy, Volume 1, pp. 13-24.
[55] Yang, Y. et al., (2014). Rotational piezoelectric wind energy harvesting using impact-induced resonance. APPLIED PHYSICS LETTERS, Volume 105, pp. 1-5.
[56] Yang, Z. & Zu, J., (2016). Comparison of PZN-PT, PMN-PT single crystals and PZT ceramic for vibration energy harvesting. Energy Conversion and Management, Volume 122, pp. 321-329.
[57] Yousry, Y. M. et al., (2018). Mechanisms for Enhancing Polarization Orientation and Piezoelectric Parameters of PVDF Nanofibers. Advanced Electronic Materials, pp. 1-8.